Mine Water Environ (2017) 36:51–58
DOI 10.1007/s10230-016-0394-4

TECHNICAL ARTICLE

Quantitative Prediction of Water Volumes Within a Coal Mine Underlying Limestone Strata Using Geophysical Methods

Cai Yang[1,2] · Shengdong Liu[1,2] · Rongxin Wu[3]

Received: 6 July 2015 / Accepted: 27 February 2016 / Published online: 19 March 2016

Abstract Mine water and mine inflow water are closely linked to the risk of mine water disasters. The relationships between various geophysical parameters and the volume of water in mine tunnels were considered by using an integrated suite of appropriate geophysical methods [i.e. direct current (DC) resistivity, transient electromagnetic method (TEM), and the seismic scattered wave method], and knowledge of the essential features of seam floor water in karst coal mine settings. By constructing a 3-dimensional physical simulation of water-bearing limestone, a quantitative predictive formula for water volume in abnormal bodies was derived in terms of the parameters of the selected suite of geophysical methods. Water volume was determined by using apparent resistivity (obtained from the DC resistivity survey and TEM), a measure of the amount of potentially water-containing space, and a correction coefficient. The quantitative formula was adjusted for accuracy using field data, and then tested at a specific field site. The average accuracy of predictions using the composite quantitative formula was 75.8 %, which is considered to be high. The formula presented in this paper could contribute significantly to the prevention and mitigation of water-related disasters in karst coal mines.

Keywords Huainan mining area in China · Physical simulation · Field test · Multi-parameter integration

Introduction

China is one of several countries faced with mitigating the threat of water-related coal mining disasters. As the average depth of coal mining in China has increased, safe production is increasingly threatened (Dong 2010; Hu ; Jin et al. 2013; Wu 2014; Wu et al. 2013; Xu et al. 2012). With greater water pressure on coal seam floors, water flowing in mining-induced fractures and mine tunnels can easily become connected to high-pressure karst water in these floors (Dong and Hu 2007). This can lead to major water inrush accidents, resulting in multiple casualties and significant economic losses. At present, efforts to prevent and mitigate major coal mine-related water inrush disasters rely on the detection, prediction, and monitoring of w2013ater inrush threats (known as the "three-detection technology") and geophysical prospecting, drilling, and chemical prospecting (Lian et al. 2014). According to Liu et al. (2014), the parameters of multi-technology should be analyzed together to predict and prevent mine water disasters.

The prediction of mine water inflow rates and the estimation of water volumes of abnormal bodies (mainly karst water and goaf water) in the vicinity of mining are important steps in determining the likely risk of mine-related water disasters. Much research has been done worldwide on the prediction of mine water inflow. The

Electronic supplementary material The online version of this article (doi:10.1007/s10230-016-0394-4) contains supplementary material, which is available to authorized users.

✉ Shengdong Liu
lsd621225@126.com

Cai Yang
yangcaicumt@163.com

[1] School of Resource and Earth Science, China University of Mining and Technology, Xuzhou 221116, China

[2] State Key Laboratory of Deep Geomechanics and Underground Engineering, China University of Mining and Technology, Xuzhou 221116, China

[3] School of Earth and Environment, Anhui University of Science and Technology, Huainan 232001, China

main approaches that have been adopted include numerical methods, analytical methods, and neural network methods (Lian et al. 2014; Yang and Chen 2009). The results yielded by these have an average margin of error of more than 200 % when compared with the actual measured data. Meanwhile, direct current (DC) resistivity and transient electromagnetic method (TEM) have proven successful in estimating water volumes in abnormal bodies (Benkabbour et al. 2004; Danielsen et al. 2003; Jiang et al. 2010; Yu et al. 2007a, b; Yue and Li 1997). However, given the multiplicity of solutions obtained with different geophysical methods, it is likely that errors will be incurred where a single method is used to estimate the amount of karst mine floor water. This could, in turn, lead to the incorrect use of these data. Geophysical mine interpretation is still in the qualitative research phase and quantitative mine interpretation studies are rare. To reduce the uncertainty associated with the application of a single predictive technology or geophysical method, this study used an integrated set of geophysical methods (the DC resistivity method, TEM, and the seismic scattered wave imaging method) to investigate the relationships between geophysical parameters and the groundwater flowing along the coal seam floor (or the water in an abnormal body). The estimates of water quantity along the coal seam were tested using the measured data. This approach should contribute considerably to the prediction of mine water inrush and the prevention and mitigation of mine water disasters.

The quantitative relationships between water volume and electrical parameters (apparent resistivity and primary field current) have been established by experimentation (Liu et al. 2010, 2013), and form the foundation for this research. Based on an integrated set of geophysical methods and a knowledge of the characteristics of groundwater in karst settings, a physical model of seam floor water in limestone was constructed. Based on this model, seam floor water volumes were quantitatively modeled in terms of geophysical parameters. This quantitative model, populated with experimental data collected in the field, was then used to predict seam floor water volumes.

Design of Physical Simulation

A physical simulation model of a coal seam was built in accordance with the theory of similarity and simulation (see Supplemental Fig. 1). Details regarding materials used in the model's construction are presented in Supplemental Table 1. A square water tank (30 cm long, 15 cm wide, and 40 cm high), representing an abnormal body, was built into the middle of the physical model. The profile lines necessary for the DC resistivity method and the receiver coils required by the TEM were embedded into the model during construction.

DC Resistivity Method

The observation system arrangement for the DC resistivity survey is shown in Supplemental Fig. 2. Lines 1 and 2 were on the edge of the model. The horizontal distance between line 1 and the water tank boundary was 18 cm, and the horizontal distance between line 2 and the water tank boundary was 28 cm. There was a height difference of 14 cm between lines 1 and 2, and 64 electrodes were mounted along each line. Each line was 126 cm long, and the distance between adjacent electrodes was 2 cm. The electrodes were made of copper wire (0.5 mm diameter). A parallel network instrument (hereafter referred to by its Chinese abbreviation, WBD (Liu et al. 2007) was used for data acquisition. WBD has two acquisition modes—AM and ABM. AM allows for the collection of all pole–pole and pole–dipole array data, whilst ABM allows for the collection of all of the four electrodes array data, such as Wenner array, dipole–dipole array and Schlumberger array. The acquisition mode selected was ABM (Liu and Zhang 2006); the duration of charge was 0.2 s, the sampling interval was 100 ms, and the service voltage was 96 V. The DC electrical survey data were collected four times: when the water tank was injected with 0, 6, 10, and 16 L of water, respectively.

Transient Electromagnetic Method

On the physical model, coils 1# and 2# were arranged symmetrically facing the water tank. Their spatial position is described in Fig. 1 (the green coil represents the receiving coil and the red coil represents the transmitting coil). A YCS 360 multichannel TEM instrument, which is manufactured in China, was used for data acquisition. The acquisition and coil parameters are presented in Tables 1 and 2. The TEM data were collected when the water tank was injected with 0, 5.71, 9.08, and 14.23 L of water, respectively.

Seismic Scattered Wave Imaging Method

The seismic survey line was 90 cm long. It was mounted on the long side of the model, 10 cm from the top. The horizontal distance from the line to the water tank was 30 cm. Head and tail sensors were placed 15 cm from either end of the line, respectively. Six adjacent sensors were glued to the side of the model at 12 cm intervals along the line. Thirty-one shot points were stimulated at 3 cm intervals from the left of the line. The observation

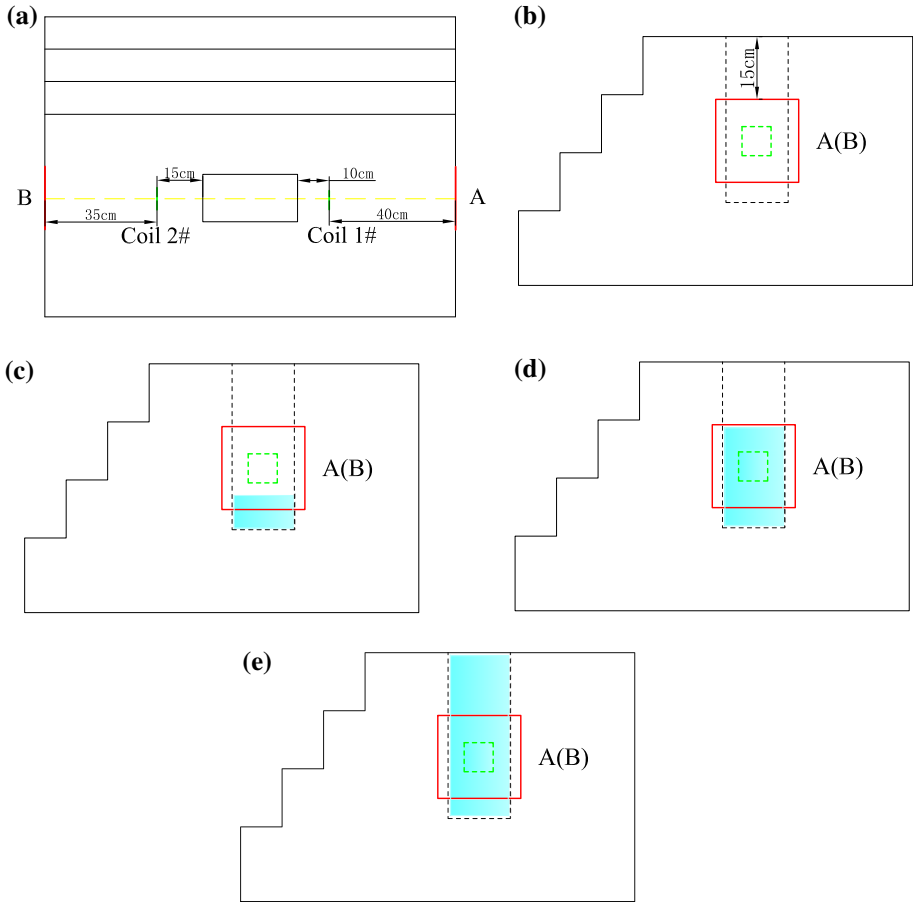

Fig. 1 Observation system arrangement with respect to transient electromagnetic method. **a** Vertical view, **b** side view, **c** first injection, **d** second injection, **e** third injection

Table 1 Acquisition parameters with respect to transient electromagnetic method

Coil 1#, 2#	No water	First injection	Second injection	Third injection
Stacking fold	1024	1024	1024	1024
Sampling frequency (MHz)	1.25	1.25	1.25	1.25
Emission current (A)	2	2	2	2
channels	40	40	40	40
Injection (g)	0	5713	3937	5148
Water quantity (L)	0.1	5.71	9.08	14.23

Table 2 Coil parameters with respect to transient electromagnetic method

	Transmitting coil (TX)		Receiving coil (RX)		Offset (cm)	Observation system
	Side-length (cm)	Number of turns	Side-length (cm)	Number of turns		
Coil 1# (observation point A)	20	10	6	30	40	Coaxial observation system
Coil 2# (observation point B)			7	30	35	

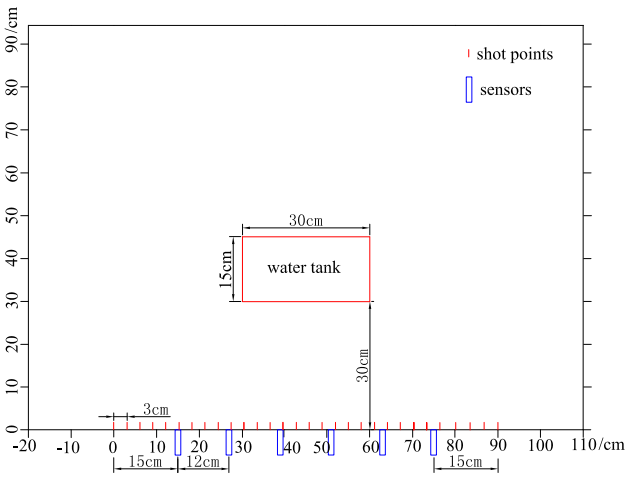

Fig. 2 The observation system arrangement with respect to seismic scattered wave imaging

system arrangement with respect to the seismic scattered wave imaging method is depicted in Fig. 2.

A DH5920N dynamic signal system was used for seismic data acquisition by a DH187 acceleration sensor. The source of the shots was a low capacity air gun. Each shot emitted the same amount of energy. The sampling frequency was 1 MHz, the sampling duration was 8 K, and the delay duration was 1 K.

Physical Model Data Analysis

Analysis of DC Resistivity Survey Data

Apparent DC resistivity was assessed at a range of tank water volumes along two lines. Mean apparent resistivity was calculated for each line spanning the cross-sectional area of the water tank. This was achieved by processing data from three different Wenner arrays (i.e. alpha, beta, and gamma). Next, it was assessed whether there was a correlation between the water volume and the apparent resistivity mean measured at the cross section of the tank (see Fig. 3). Analysis of the data for both lines 1 and 2 revealed that as the water volume increased, the apparent resistivity mean gradually decreased. Through mathematical fitting, the relationship between water volume and the apparent resistivity mean can be expressed as follows:

$$\rho_{s1} = -a_1 \cdot \ln Q + b_1 \quad (1)$$

where ρ_{s1} (Ω·m) is the apparent resistivity mean obtained through the DC resistivity survey, Q (ml) is the volume of water in the tank, and a_1 and b_1 are constants. For the physical simulation, $a_1 = 1.256$–3.837, and $b_1 = 46.185$–99.216, with $R^2 = 0.3868$–0.8429.

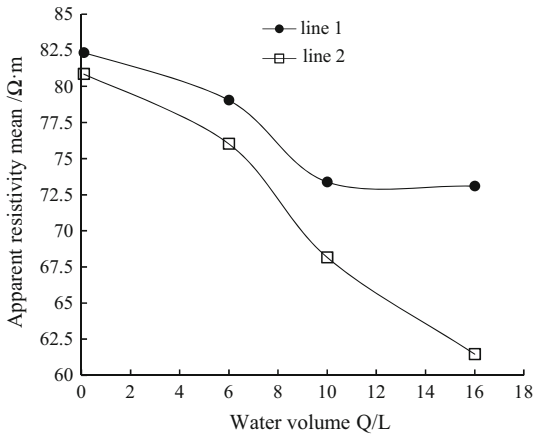

Fig. 3 Water volume versus apparent resistivity mean according to DC resistivity survey

Analysis of Data Obtained Through the Transient Electromagnetic Method

Figure 4 depicts the induced voltage decay curves for the secondary fields of coils 1# and 2#. We found that the induced voltages were at a minimum when the water tank contained no water, and after $t = 342.4$ μs. As the volume of water in the tank increased, the induced voltage decay curves for the secondary fields of both coils 1# and 2# gradually escalated. The increased amplitude of the curve

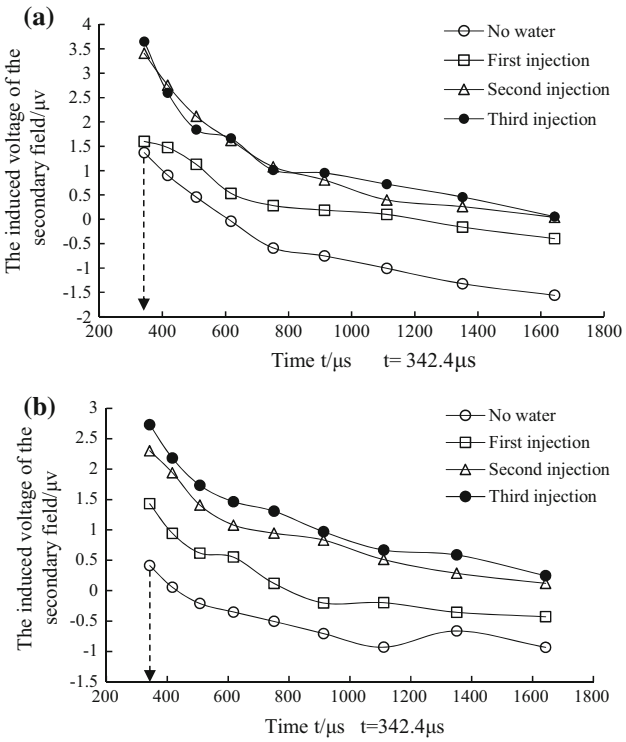

Fig. 4 The induced voltage decay curves for the secondary fields of coil 1# and coil 2#. **a** Coil 1#. **b** Coil 2#

with respect to coil 2# was slightly more marked than that for coil 1#, which implies that the induced voltage of the secondary field of coil 2# was more sensitive to a change in water volume.

The variation characteristics of the induced voltage decay curves at points A (coil 1#) and B (coil 2#) were essentially consistent. The induced voltages for observation point B were obtained when the water tank contained no water, and then when it contained 5.7135, 9.0835, and 14.2315 L of water, respectively.

Late-time apparent resistivity values at t1, t2, and t3 were calculated and compared (see Fig. 5). By mathematical fitting of the curve in Fig. 5, the relationship between water volume and the apparent resistivity mean can be expressed as follows:

$$\rho_{s2} = -a_2 \cdot \ln Q + b_2 \quad (2)$$

where ρ_{s1} (Ω m) is the apparent resistivity mean obtained through the TEM, Q (mL) is the volume of water in the tank, and a_2 and b_2 are constants. For the physical simulation, $a_2 = 2.72$–4.39, and $b_2 = 26.50$–39.87, with $R^2 = 0.737$–0.851.

Analysis of Data Obtained Using the Seismic Scattered Wave Imaging Method

Analyzing wave migration for a common scattering point is mainly applied in the seismic scattered wave imaging. In theory, as long as the seismic record is long enough, the energy of any scattering point in the detection region can be found in any of the channels according to the travel time of its propagation. In exploring scattered wave migration for common scattering points, the detection region is discretized into a grid with cells representing scattering points. The energy of different seismic track records is classified into the grid according to corresponding scattering imaging points, forming the scattered migrated-superimposed signal (Fig. 6).

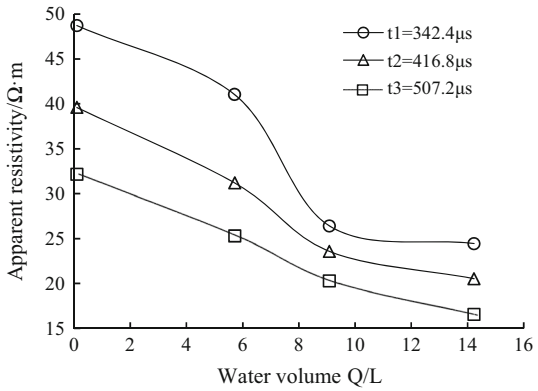

Fig. 5 Water volume versus apparent resistivity for coil 2# (at t_1, t_2, and t_3)

Fractured zones and water-rich areas are often accompanied by changes in lithology. Thus, the scattered migrated-superimposed signals were reprocessed by adopting the relative extremum method, which is used to delineate anomaly boundaries. The scattered migrated-superimposed signals were considered according to their amplitudes in the horizontal direction (prospecting length) and the vertical direction (depth), respectively. The amplitude of every signal (where energy exceeded a fixed threshold) was obtained. The relative extremum relationships between gathers were compared in the horizontal direction, simultaneously, to demarcate the anomaly boundary.

For Fig. 6, the energy threshold was set at 20 % of the maximum energy of each gather signal. In the range of 0–1 ms, the amplitude was registered for each signal when it exceeded this threshold. Each 1 ms signal was divided into ten units of 0.1 ms each. Amplitudes were recorded for each of these 0.1 ms time windows. To eliminate the effects of direct waves, extreme values were normalized. The abnormal body's boundary delineated by the relative extremum method (where the relative extreme value was >4) is displayed as Fig. 7.

Integrated Geophysical Modeling

From data obtained through the physical simulation exercise, a composite and integrated water volume prediction formula was derived by integrating the relationships and patterns revealed by each of the geophysical methods employed in the simulation (i.e., DC resistivity survey, the transient method, and the seismic scattered wave imaging method).

1. DC resistivity method:

$$Q = e^{\frac{b_1}{a_1} - \frac{1}{a_1} \cdot \rho_{s1}} \quad (3)$$

where Q is the water volume and ρ_{s1} is the apparent resistivity (where $a_1 = 1.256$–3.837, $b_1 = 46.185$–99.216), with $R^2 = 0.3868$–0.8429.

2. Transient electromagnetic method:

$$Q = e^{\frac{b_2}{a_2} - \frac{1}{a_2} \cdot \rho_{s2}} \quad (4)$$

where Q is the water volume and ρ_{s2} is the apparent resistivity (where $a_2 = 2.72$–4.39, $b_2 = 26.50$–39.87), with $R^2 = 0.737$–0.851.

3. Seismic scattered wave imaging method: the abnormal energy of scattered seismic waves can provide the basis for the delineation of water-bearing spaces. Where lithology is constant, the energy of scattered seismic waves can be used to reveal the existence and extent of abnormal bodies. Using the relative extremum method, the two-dimensional space of abnormity was obtained.

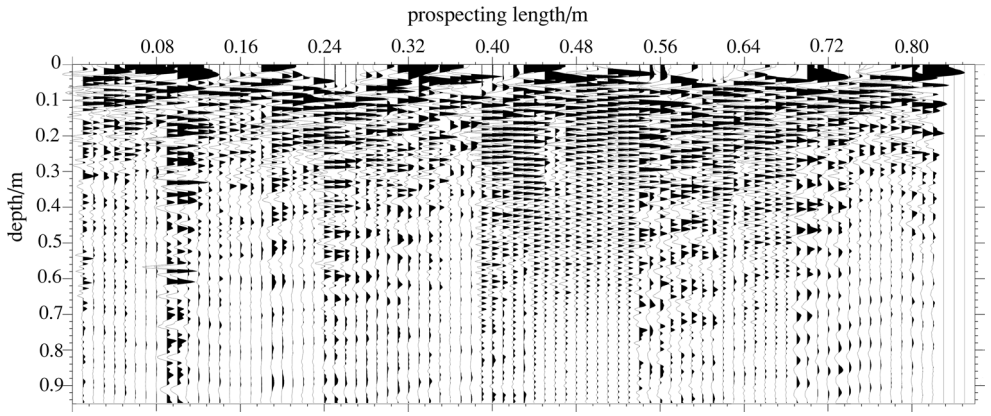

Fig. 6 Superimposed signals of scatter migration

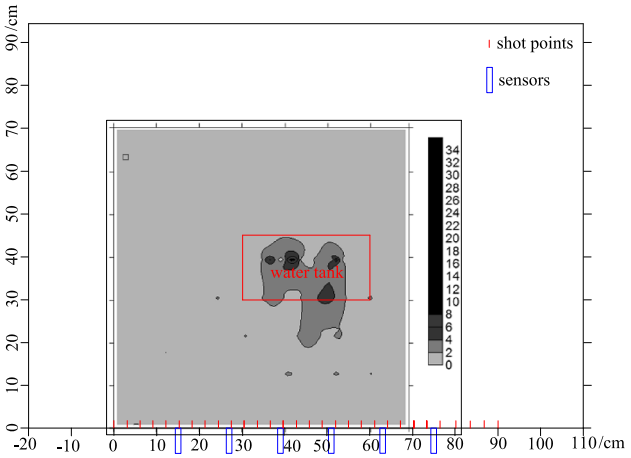

Fig. 7 Abnormal body's boundary delineated according to the relative extremum method

4. The rule of multi-parameter integration: First, there is an exponential relationship between water volume and the apparent resistivity measurements obtained through the DC resistivity method and TEM. Also, rock resistivity is closely related to moisture content and the number/extent of fissures in it. Thus, $e^{a+b\cdot\rho_s}$ expresses rock moisture content, where ρ_s is the composite apparent resistivity based on the resistivity measurements obtained through the DC resistivity method and the TEM. The contribution of each of these methods is weighted according to the actual characteristics of a particular mine. This is because that the electrical parameters of the DC resistivity method and the TEM are more sensitive to mine water.

Second, water-containing spaces between crack boundaries in rock strata can be delineated as "abnormal spaces" based on the boundary features of the abnormal energy of seismic scattered waves. Not all cracks are water-containing areas. Low resistivity areas identified by the DC resistivity survey and the transient electromagnetic method could also be explained by changes in mineral composition or particular lithology (such as mudstone) of rock strata. Therefore, the effective water-containing spaces are defined as those where seismically detected "abnormal space" and electrically delineated low resistivity areas overlap.

According to the abovementioned rules of multi-parameter integration, an integrated water volume prediction formula can be expressed as follows:

$$Q = k \cdot e^{a+b\cdot\rho_s} \cdot V \tag{5}$$

where Q (m^3) is water volume and k is the correction coefficient determined by water inflow data in mine experimental section (the default is 1); $e^{a+b\cdot\rho_s}$ is the rock moisture factor (a and b are constants determined by experimental conditions); V represents water-containing space determined by $V_{SS} \cap (V_{DC} \cup V_{TEM})$,which is the intersection of crack areas identified through seismic detection and low resistivity areas delineated by the DC resistivity and transient EM methods. Where seismic data is lacking, V mainly relies on $V_{DC} \cup V_{TEM}$.

Project Application

Derivation of Formula Constants from Field Data

Because of inevitable differences between the laboratory-based physical model and actual geological settings, the unknown parameters of the water volume prediction formula described above were determined using data collected in the field, with the hope of improving the overall accuracy of the quantitative model. Thus, parameters a and b were derived using data collected in a mine in the Huainan mining area between 2011 and 2012.

A DC resistivity survey of a limestone water discharge channel at a depth of 490 m was completed in March 2011.

Very little groundwater drainage had been done at that stage, which meant that the low resistivity areas identified by this survey constituted a reliable reflection of true water-bearing zones in the limestone matrix. Seismic data were collected in 2012, but the time difference is considered negligible as seismic survey results of abnormal body's boundary are not significantly influenced by changes in water discharge. A TEM survey was also completed in 2012, but its results were seriously affected by water discharge, and were thus not considered suitable for use in deriving a composite water volume prediction formula. Thus, the water-containing space V was determined using the results of only the DC electrical resistivity survey and the seismic scattered wave method.

The relationship between the three-dimensional water-containing space and the two-dimensional cross-sectional area S is calculated as follows (assuming that the water-containing space is a sphere):

$$V \approx S^{2/3} \tag{6}$$

where V is the water-containing area and S is the cross-sectional area.

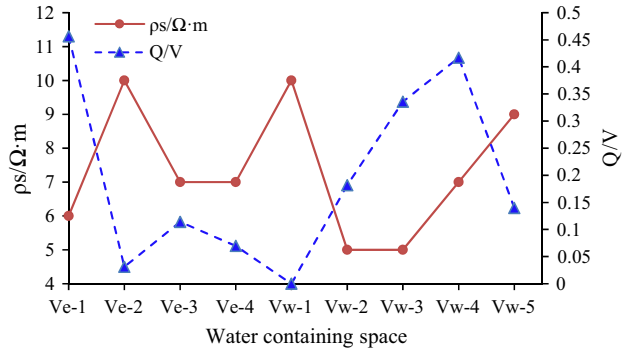

Fig. 8 Q/V and apparent resistivity of groundwater discharge channel measured in the field

Nine water-containing areas were delineated in the field study. After calculating the mean apparent resistivity (according to the DC resistivity survey method) of the water-containing areas, the following integrated water volume prediction formula was derived:

$$Q = k \cdot e^{0.69704 - 0.363\rho_s} \cdot V \tag{7}$$

where Q (m^3) is water volume, ρ_s (Ω m) is apparent resistivity, and k is a correction constant. Figure 8 shows the graph of $Q/QV.V$and the apparent resistivities of the nine water-containing spaces identified along the 490-m-deep groundwater discharge channel. The marks Ve-1, Ve-2, Ve-3, Ve-4, Vw-1, Vw-2, Vw-3, Vw-4, and Vw-5 stand for the names of different water-containing space in Fig. 8.

Testing of the Quantitative Model

Using Eq. 7, the water volumes of six abnormal water-containing areas along the east limestone water discharge tunnel (at a depth of 580 m) were predicted. Because of the influences of water discharge, the resistivity of the discharge tunnel at a depth of 490 m was less than that of the tunnel at a depth of 580 m east of the limestone water discharge roadway. Thus, the water volumes predicted for the −580 m section were generally inflated, leading to an adjustment of the correction coefficient to $k = 0.25$. Table 3 shows the parameters used to predict the water volumes of water-bearing areas along the −580 m eastern limestone water discharge roadway. The predicted water volumes were consistent with actual groundwater inflows, and agree with actual measured water volumes. The average accuracy of the predicted water volumes was 75.8 %. A comparison of the predicted and actual water volumes (Q_P and Q_0) is presented in Fig. 9.

Table 3 Parameters used to predict water volumes of abnormal bodies along the −580-m eastern limestone water discharge roadway

Water-containing space	S (m^2)	V (m^3)	ρ_s (Ω m)	Drill	Water flow (m^3)	Q_0 (m^3)	Q_p (m^3)
D-0	900	27,000	7	E0-1	120	1100	1067
				E0-2	70		
				E0-3	10		
				E0-4	900		
D-1	800	22,627	12	E1-2	0	0	146
D-2	1600	64,000	9	E5-1	1800	1800	1224
D-3	1000	31,622	9	E5-2	60	440	605
				E5-3	120		
				E6-3	260		
D-4	1000	31,622	9	E7-1	0	0	605
D-6	1200	41,569	6	E10-2	1500	1500	2362

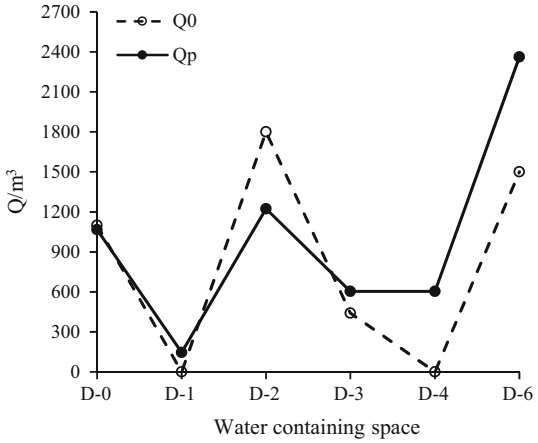

Fig. 9 Comparison between predicted and actual water volumes (Q_P and Q_0)

Conclusion

In summary, this paper presents a method to quantitatively predict mine water inflow and water volumes in abnormal bodies. This new integrated approach takes the form of a quantitative model derived through multi-parameter integration following the simultaneous application of several relevant geophysical methods. It is important to adjust the predictive formula based on field data for a specific site, because the valid application region of the equation is limited by mine geology characteristics. The experimental apparatus should be improved and modified in the future by accounting for the complex geological conditions of the mine. It is necessary to consider the influences of lithological variations, such as fractures, porosity, and mineral composition. The comprehensive geophysical characteristics of coal, sandstone, mudstone, and limestone, which are affected by mine water, should also be analyzed and compared. Comprehensive geophysical modeling is mainly depended on the detection of floor limestone water in the Huainan mining area. The quantitative formula should be further corrected when used in other mining areas based on the specific geological conditions. It would also be good to improve the design of the physical model to maximize the applicability of the theoretical prediction formula derived from it.

Acknowledgments We gratefully acknowledge financial support by the National Natural Science Foundation Projects, "Detecting Theory and Method of High Resolution Mine Seismic Detection" (Grant No. U1261202).

References

Benkabbour B, Toto EA, Fakir Y (2004) Using DC resistivity method to characterize the geometry and the salinity of the Plioquaternary consolidated coastal aquifer of the Mamora plain, Morocco. Environ Geol 45(4):518–526

Danielsen JE, Auken E, Jørgensen F, Søndergaard V, Sørensen KI (2003) The application of the transient electromagnetic method in hydrogeophysical surveys. J Appl Geophys 53(4):181–198

Dong S (2010) Some key scientific problems on water hazards frequently happened in China's coal mines. J Chin Coal Soc 35(1):66–71 **(in Chinese)**

Dong S, Hu W (2007) Basic characteristics and main controlling factors of coal mine water hazard in China. Coal Geol Explor 35(5):34–38 **(in Chinese)**

Hu W (2013) Study orientation and present status of geological guarantee technologies to deep mine coal mining. Coal Sci Technol 41(8):1–5, 14 **(in Chinese)**

Jiang Z, Yue J, Yu J (2010) Experiment in metal disturbance during advanced detection using a transient electromagnetic method in coal mines. Min Sci Technol 20(6):861–863 **(in Chinese)**

Jin D, Liu Y, Liu Z, Cheng J (2013) New progress of study on major water inrush disaster prevention and control technology in coal mine. Coal Sci Technol 41(1):25–29 **(in Chinese)**

Lian H, Xia X, Xu B, Xu H, Yi S (2014) Evaluation and applicability study on prediction methods of water inflow in mines. J N China I Sci Technol 11(2):22–27 **(in Chinese)**

Liu S, Zhang P (2006) Signal acquisition method of electrode potential difference in the distributed paralleling intellective way. China Patent of Invention: zl200410014020.0

Liu S, Liu S, Wu R, Zhang P, Fan Y (2007) Network parallel electrical instrument and stationary electrical prospecting. China Sci Technol Achiev 7(24):31–36 **(in Chinese)**

Liu S, Yang S, Cao Y, Liu J (2010) Analysis about response of geoelectric field parameters to water inrush volume from coal seam roof. J Min Safety Eng 27(3):341–345 **(in Chinese)**

Liu J, Liu S, Cao Y, Yang S (2013) Quantitative study of geoelectric parameter response to groundwater seepage. Chin J Rock Mech Eng 32(5):986–993 **(in Chinese)**

Liu SD, Liu L, Yue J (2014) Development status and key problems of Chinese mining geophysical technology. J China Coal Soc 39(01):19–25 **(in Chinese)**

Wu Q (2014) Progress, problems and prospects of prevention and control technology of mine water and reutilization in China. J China Coal Soc 39(5):795–805 **(in Chinese)**

Wu Q, Cui F, Zhao S, Liu S, Ceng Y, Gu Y (2013) Type classification and main characteristics of mine water disasters. J China Coal Soc 38(4):561–565 **(in Chinese)**

Xu J, Liu S, Wang B, Zhang P, Gui H (2012) Electrical monitoring criterion for water flow in faults activated by mining. Mine Water Environ 31:172–178

Yang Y, Chen Y (2009) Chaotic characteristics and prediction for water inrush in mine. Earth Sci J China Univ Geosci 34(2):258–262 **(in Chinese)**

Yu J, Liu Z, Yue J, Liu S (2007a) Development and prospect of geophysical technology in deep mining. Prog Geophys 22(2):586–592 **(in Chinese)**

Yu J, Liu Z, Liu S, Tang J (2007b) Theoretical analysis of mine transient electromagnetic method and its application in detecting water burst structures in deep coal stope. J China Coal Soc 32(8):818–821 **(in Chinese)**

Yue J, Li Z (1997) Mine DC electrical methods and application to coal floor water invasion detecting. J China Univ Min Technol 26(1):94–98 **(in Chinese)**